RSC Advances

PAPER

View Article Online
View Journal | View Issue

Cite this: *RSC Adv.*, 2017, **7**, 16826

Investigation of the post-annealing electromagnetic response of Cu–Co oxide coatings *via* optical measurement and computational modelling†

M. Mahbubur Rahman,[ab] Hussein A. Miran,[ac] Zhong-Tao Jiang,*[a] Mohmmednoor Altarawneh,[d] Lee Siang Chuah,[e] Hooi-Ling Lee,[f] Amun Amri,[g] Nicholas Mondinos[a] and Bogdan Z. Dlugogorski[d]

Received 21st October 2016
Accepted 3rd March 2017

DOI: 10.1039/c6ra25626k

rsc.li/rsc-advances

The optical frequency response and changes to the dielectric and optical parameters due to annealing temperature variation (200–500 °C) of sol–gel derived $CuCoO_x$ thin film coatings were investigated. The optical constants such as absorption coefficient, band-gaps, Urbach energy, complex refractive index, complex dielectric constants, optical dispersion parameters, and energy loss functions were determined from reflectance data analysis recorded in the ultraviolet to near-infrared (190–2200 nm) range. The absorption coefficient and the broadening of absorption edge (steepness parameter), energy band-gaps, Urbach energy, loss tangent and energy loss functions decreased with the increase in annealing temperatures. The refractive index displayed normal dispersion behaviors at higher frequency with the maximum value at a temperature of 500 °C. First-principles simulations, density functional theory (DFT+U) as implemented in the Cambridge Serial Total Energy Package (CASTEP), based on a cluster structure of $Cu_{0.5}Co_{2.5}O_4$ system, optimized the crystalline structure and calculated the electronic structure of the framework. The calculated density of states (DOS) and associated absorption coefficient and dielectric constant results reasonably support the experimental findings.

1. Introduction

Mixed metal oxide based coatings with general composition AB_2O_4, where A is a divalent metal ion occupying the tetrahedral A-sites, and B is a trivalent ion occupying at octahedral B-sites, *e.g.*, $CuFe_2O_4$, $CuCo_2O_4$, and $CuMn_2O_4$, have been extensively studied by different groups.[1–4] These materials possess widespread applications as catalysts for volatile organic compounds,[5] gas sensors,[6] electrocatalysts for the oxygen electrode,[7] photovoltaics and photocatalysis,[8] selective solar absorbers,[9,10] batteries and memory devices,[11,12] and for absorption optimizations and industrial applications.[13] High-tech applications of cobalt based metal oxide coatings are demonstrated in the literature.[11,12,14,15] Pure copper oxide,[16] cobalt–copper oxide, manganese–cobalt oxide, nickel–cobalt oxide,[13] copper–aluminum oxide[17,18] have been reported in studies of spectrally selective solar absorbers, high absorption optical coatings and industrial applications. Manganese-cobalt oxides have been studied with a focus on the influence of synthesis conditions on the oxidation states and cationic distribution in the tetragonal and cubic phases.[19] Optical characterization of industrial roll-coating sputtered nickel–nickel oxide solar selective surface has been reported by Adsten *et al.*[20] Structural and optical properties of pulsed sputter deposited $Cr_xO_y/Cr/Cr_2O_3$ solar selective coatings on Cu substrates were found to demonstrate high selectivity after being annealed at 300 °C for 2 hours in air.[21] In another study, Shaklee *et al.*[22] examined the spectral selectivity of composite enamel coatings consisting of spinel-type transition-metal-oxide pigments embedded in a borosilicate-glass matrix deposited on stainless steel substrate.

The cobalt oxide (Co_3O_4) films containing 1-D interlinked nanowires synthesized *via* spray pyrolysis technique showed better values of absorptance (0.94), emittance (0.17) compared

[a]*Surface Analysis and Materials Engineering Research Group, School of Engineering & Information Technology, Murdoch University, Murdoch, Western Australia 6150, Australia. E-mail: Z.Jiang@murdoch.edu.au; Tel: +61 8 9360 2867*

[b]*Department of Physics, Jahangirnagar University, Savar, Dhaka 1342, Bangladesh*

[c]*Department of Physics, College of Education for Pure Sciences, Ibn Al-Haitham, University of Bagdad, 10071, Baghdad, Iraq*

[d]*School of Engineering & Information Technology, Murdoch University, Murdoch, Western Australia 6150, Australia*

[e]*Department of Physics, School of Distance Education, Universiti Sains Malaysia, 11800 Minden, Penang, Malaysia*

[f]*School of Chemical Sciences, Universiti Sains Malaysia, 11800 Minden, Penang, Malaysia*

[g]*Department of Chemical Engineering, Universitas Riau, Pekanbaru, Indonesia*

† Electronic supplementary information (ESI) available. See DOI: 10.1039/c6ra25626k

to the data reported studies. The selectivity of coatings was reported to be 5.529. These coatings have the potential of being good selective absorbers. Their optical properties indicate the red shift of absorption peaks, thereby showing a quantum-confined effect and semiconducting nature.[23] In Amun's study,[24] the combined CuCoO thin films showed a selectivity of just over 14. There have been numerous investigations available in studies on metal oxide thin films for the improvement and optimization of physiochemical, optical, thermal, electrochemical, photo-chemical, magnetic, dielectric and electromagnetic properties focusing on their practical applications such as clean energy devices, solar cells, photovoltaics, thermal collectors, selective solar surfaces and smart windows.

In view of these facts, generally, the optical analyses of materials are mainly involved with the absorption, reflection, emission and transmission measurements in the ultraviolet through visible to infrared and far-infrared regions of the solar spectra to realize their solar absorptance mechanisms and solar selectivity topographies. It is also seen, there has been very limited effort toward elucidating the post annealing effects on the other properties of these coatings. Optical characterizations of these materials play remarkable roles to comprehend their fundamental behaviors and make them preferable in several applications. However, using the optical data, we can conduct further studies *e.g.*, optical dispersion analyses, dielectric features and energy loss phenomena that afford them with the identification of their potentiality in the new promising extents to be used more competently. Thus, in this study, we have carried out detailed studies to understand the post-annealing electromagnetic responses of energy band-gaps, single oscillator model optical dispersion analysis, dielectric characterizations, and energy loss mechanisms of sol–gel derived copper–cobalt oxide coatings.

2. Experimental and modeling

2.1 Specimen synthesis

Cobalt(II) chloride ($CoCl_2 \cdot 6H_2O$, APS Chemical, >99%), copper(II) acetate monohydrate ($(Cu(OOCCH_3))_2 \cdot H_2O$, Alfa Aesar, >98%), propionic acid (C_2H_5COOH, Chem Supply, >99%), and absolute ethanol (E. Mark of Germany, >99%.) were used to synthesize CuCo-oxide coating onto highly-reflective commercial aluminium substrates. The aluminium substrates (Anofol, size 2 cm × 4 cm) were cleaned with a hot mixture of chromium(VI) oxide and phosphoric acid followed by final rinse using Milli-Q water. The cleaned substrates were dried with high purity N_2 gas. The sol–gel solutions consisted of 1.502 gm cobalt(II) chloride ($CoCl_2 \cdot 6H_2O$, 0.25 mol L^{-1}) and 1.273 gm of copper(II) acetate monohydrate ($(Cu(OOCCH_3))_2 \cdot H_2O$ mixed with absolute ethanol. Propionic acid (C_2H_5COOH) was used to make a complex solution with the metal ions and to stabilize the solution from unwanted precipitation. After stirring the mixed solution for 2 h, the sol was coated onto aluminium substrates using a dip-coating technique. A dipping and withdrawal rate of 180 mm min^{-1} and 60 mm min^{-1}, respectively was maintained throughout the synthesis process which was repeated four times to increase the thickness of film with better uniformity. Finally, the coatings were annealed at 200, 300, 400 and 500 °C in air. A constant heating rate of 10 °C min^{-1} was maintained throughout and the samples were left in the furnace for 15 min after power was turned off. More details about the sol–gel dip-coating method are described elsewhere.[18,24–26]

2.2 Characterization techniques

A UV-Vis (UV-670 UV-Vis spectrophotometer, JASCO, USA) double beam spectrophotometer with 60 mm integrating sphere was used to record the UV-Vis reflectance spectra in the range of 190 to 2200 nm. The UV-Vis reflectance spectrum was utilized to investigate the various characteristics of the copper–cobalt oxide thin films.

2.3 Density functional theory

First-principles calculation is one of the most promising approaches to predict the ground state properties of a material. The XRD results from Miran *et al.*[27] revealed that the adopted phase for this coating material, as annealing temperature progress within the same range of temperatures is, $Cu_{0.56}Co_{2.44}O_4$. The $Cu_{0.5}Co_{2.5}O_4$ system was dealt with the level of density functional theory (DFT+U) proposed by Dudarev *et al.*[28] as implemented in the Cambridge Serial Total Energy Package (CASTEP)[29,30] of Material Studio. For the interactions of the electrons with the ion cores, a plane wave and non-local ultra-soft pseudopotentials presented by Vanderbilt[31] have been applied together with the generalized-gradient approximation (GGA).[32] The electronic wave functions are expanded in a plane wave basis set with an energy cutoff of 351 eV. For the Brillouin-zone *k*-point sampling, we adopted the Monkhorst–Pack mesh with 4 × 4 × 4 *k*-points. Finally, the electron-correlated systems (*i.e.*, d-orbital) were modeled considering Hubbard *U* value of 9.5 eV that leads to a well agreed band gap with experiment measurements.

3. Results and discussion

3.1 Structural and morphological features of Cu–Co oxide coatings before and after annealing

Structural and morphological analyses of these coatings carried out *via* XRD, XPS, FESEM and AFM spectroscopic methods, before annealing and after annealing, were reported in our most recent studies.[27] Before annealing the CuCo-oxide coatings, FESEM showed mould-like structures. However after thermal treatment homogeneously distributed particles with compact and smooth morphologies were observed. The mean and rms surface roughness of the coatings improved ~120% and ~140%, respectively, with an average surface area of ~115 μm^2. Annealing results in the occurrence of major grain growth around the coating surface.[27]

XRD studies attributed that the Cu–Co oxide coatings possesses the cubic symmetry consisting of $Cu_{0.95}Co_{2.05}O_4$ (ICSD 78-2177), $Cu_{0.75}Co_{2.25}O_4$ (ICSD 78-2176), $Cu_{0.56}Co_{2.44}O_4$ (ICSD 78-2175), and $Cu_{0.37}Co_{2.63}O_4$ (ICSD 78-2174) phases. In the $Cu_{0.75}Co_{2.25}O_4$ system (space group $Fd\bar{3}m$ (227), $Z = 8$, lattice parameter 0.809 nm) the unit cell consists of 6 copper atoms, 18 cobalt atoms and 32 oxygen atoms. Copper and cobalt atoms are

shared in tetrahedral and octahedral sites. Fig. 1 shows the spinel structure of Cu–Co oxide system drawn using GaussView 5.0.8 software.

3.2 Electronic structure and Urbach energy studies

The dependence of optical absorption coefficient on the photon energy is useful for studying the band structure and the types of electron transition involved in absorption process. The linear absorption coefficient can be determined by using the reflectance spectra of the films *via* following relation,

$$\alpha = 2.3026\frac{A}{d} \quad (1)$$

where α is the absorption coefficient, A is the solar absorptance (in terms of %) as estimated from the UV-Vis reflectance data, and d is the coating's thickness which was obtained from FESEM measurement.[27] Fig. 2 shows the incident photon energy dependence of the absorption coefficient of sol–gel derived Cu–Co oxide coatings before and after annealing. The wavelength of light that a material absorbs is the characteristic of its chemical assembly. Specific regions of the electromagnetic spectrum are absorbed by exciting specific types of molecular and atomic motion to higher energy levels. Absorption of ultraviolet and visible light is related with the excitation of electrons, both in atoms and molecules, to higher energy states.

In crystalline and amorphous materials the photon absorption obeys the Tauc relation,[33–36]

$$\alpha h\nu = B(h\nu - E_g)^y \quad (2)$$

where, α is the absorption coefficient, $h\nu$ is the incident photon energy, h is Planck's constant, ν is the frequency of incident light, B is an energy independent constant, E_g is the optical band-gap and y is an index depending on the type of optical transition involved in photon absorption. The indices of $y = 1/2$ and 2 are for the direct and indirect inter-band transitions, respectively. The direct transition energy gap (direct band-gap) can be obtained by plotting $h\nu$ *vs.* $(\alpha h\nu)^2$ and extrapolating the linear portion of the curve to $(\alpha h\nu)^2 = 0$ in the x-axis. Similarly, the indirect energy band-gap can be estimated by plotting $h\nu$ *vs.* $(\alpha h\nu)^{1/2}$ and extrapolating the linear portion of the curve to $(\alpha h\nu)^{1/2} = 0$ in the photon energy axis.

Tauc plots of $(\alpha h\nu)^2$ *vs.* $h\nu$ for Cu–Co oxide coatings before and after annealing are shown in Fig. 3. The energy band-gaps estimated from the intercepts of the linear portion of the curves extrapolated to zero in the photon energy axis are presented Table 1. The values of direct and indirect transition energy gaps lie between 0.80 and 1.40 eV. It is found that the energy band-gap values are monotonically reduced with the rise in annealing temperature of the Cu–Co oxide systems. This drop of energy band-gap values is very important in enhancing the photon absorption capability of these coatings.

The spectral absorption in materials strongly depends on the presence of localized states around the forbidden band gap. The absorption profiles offer valuable information on these localized states and indicate the presence of disorderness in the films. Since, Urbach's absorption edges are, normally, formed in the region of photon energies below the forbidden band gaps *i.e.*, in regions of the so-called Urbach tails, where the absorption coefficient follows an exponential decay for decreasing the incident photon energy, and is expressed as,

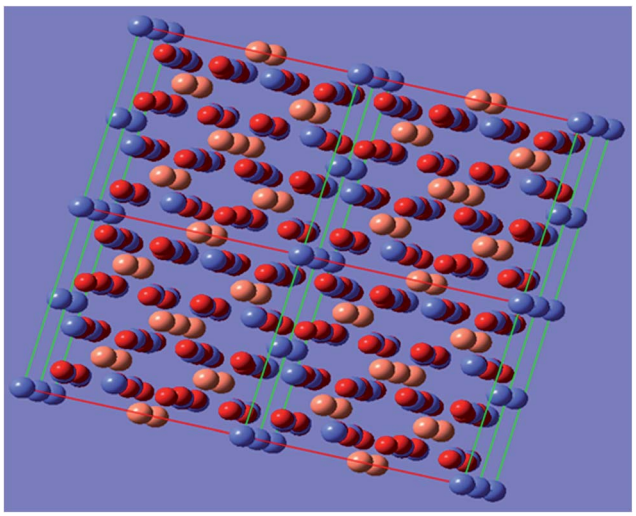

Fig. 1 Crystal structure of Cu–Co oxide coatings.

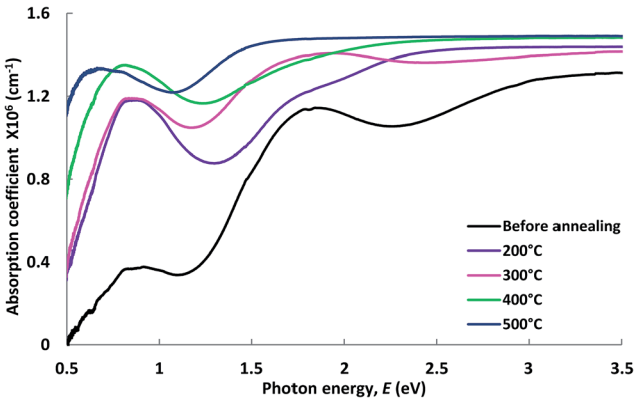

Fig. 2 Absorption coefficient of Cu–Co oxide coatings before and after annealing at different temperatures.

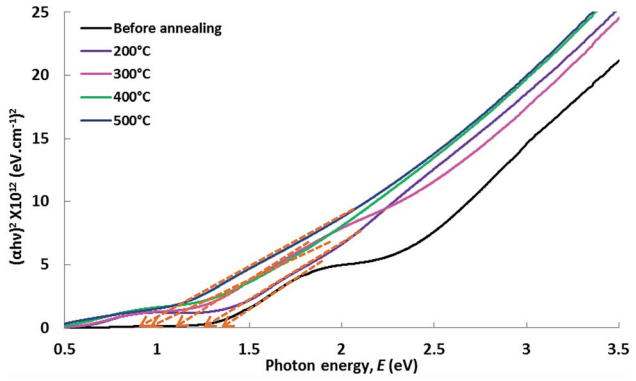

Fig. 3 Tauc plots of $(\alpha h\nu)^2$ *vs.* photon energy of Cu–Co oxide coatings before and after annealing.

Table 1 Energy band-gaps of Cu–Co oxide coatings before annealing and at different annealing temperatures

Annealing temperature	Energy band-gap, E_g (eV)
Prior-annealing	1.40
200 °C	1.35
300 °C	1.20
400 °C	0.90
500 °C	0.80

$$\alpha(h\nu) = \alpha_0 e^{\left(\frac{h\nu}{E_U}\right)} \quad (3)$$

where α_0 is a constant and E_U is the Urbach energy referring to the width of the exponential absorption edge. The value of E_U has been assessed by the exponential fitting of the sub-band-gap absorption coefficient which is the inverse of the slope of ln(α) *vs.* photon energy plots (see Fig. 4). The estimated values of E_U are illustrated in Table 2. The Urbach energy values are significantly decreased with the increase in annealing temperature of the films. This feature is consistent with the results given by Xue *et al.*[37] The reduction in E_U values are, generally, governed by the diminution of the localized density of states around the tails of the absorption edges, increase in crystallinity, decrease in the degree of disorderness and a relaxation of the distorted bonds. A reduction in Urbach energy also indicates the improvements of the films quality. A decline in E_U values of thermally evaporated films with increasing annealing temperature is consistent with our energy band-gap studies where the E_g values are also dropped with the rise in annealing.

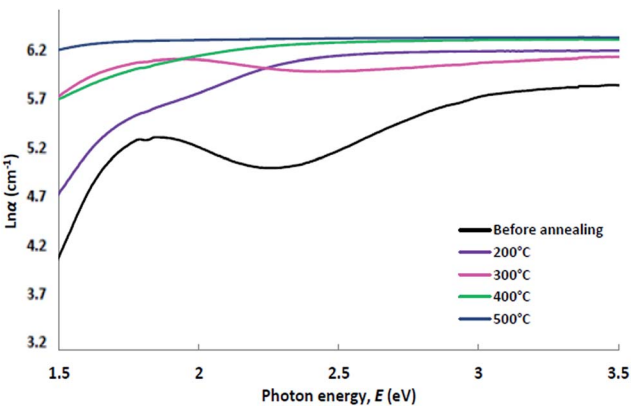

Fig. 4 Variation of ln α with photon energy of Cu–Co oxide coatings before and after annealing at different temperatures.

Table 2 Urbach energy values and steepness parameters of Cu–Co oxide coatings before annealing and at different annealing temperatures

Annealing temperature	Urbach energy, E_U (meV)	Steepness parameter, γ
Prior-annealing	500	0.0514
200 °C	400	0.0643
300 °C	318	0.0801
400 °C	267	0.0963
500 °C	188	0.1367

The spectral dependence of the absorption coefficient with the incident photon energy might arise originate from trapping levels around the film boundaries. According to Tauc's theory the density of these states fall off exponentially with the photon energy by the following relation,

$$\alpha = \alpha_0 \exp\left(\frac{\gamma h\nu}{k_B T}\right) \quad (4)$$

where γ is a constant known as the steepness parameter which refers to the broadening of absorption edges arising from electron–phonon or exciton–phonon interactions. From eqn (4), the steepness parameter, γ can be expressed as,

$$\gamma = \frac{k_B T}{E_U} \quad (5)$$

Estimated values of the steepness parameters are shown in Table 2. From Table 2, it is seen that the steepness of the Urbach band tails linearly increase with the increase in annealing temperatures. An increase in the steepness parameter originates from the diminution of the localized density of states, relaxation of the distorted bonds and thereby the degree of crystallinity of the films is enhanced. These features also support the consistency of our energy band-gap and Urbach energy studies. It is well known that the optical band structure and optical transitions are sturdily influenced by the width of the localized states around the band gaps of the films. The absorption coefficient near the fundamental absorption edge is exponentially dependent on the photon energy and obeys the Urbach rule. Interactions between lattice vibrations and localized states in tail of the band-gap of the films have a substantial consequence on the optical properties of these films.

3.3 Optical properties – parameters and dispersions

Using the UV-Vis reflectance spectra, the optical constants such as the refractive index (n) and the extinction coefficient (k) of the films were computed in the wavelength range of 190–2200 nm. The complex refractive index, an important optical parameter that is used to elucidate other materials' properties, is defined as,

$$n^* = n + ik \quad (6)$$

The imaginary part of the complex refractive index, the extinction coefficient (k) can be directly calculated from the absorption coefficient *via* following relation,

$$k = \frac{\alpha\lambda}{4\pi} \quad (7)$$

The refractive index n is calculated from the UV-Vis reflectance data, R and k values using the following equation,

$$n = \left(\frac{1+R}{1-R}\right) + \sqrt{\frac{4R}{(1-R)^2} - k^2} \quad (8)$$

where R is the reflectance (%), and k extinction coefficient of Cu–Co oxide coatings. The wavelength dependence of the refractive index, n and extinction coefficient, k values of Cu–Co oxide coatings before and after annealing at different temperatures are shown in Fig. 5.

Analysis of Fig. 5 indicates that both the values of n and k significantly increased with the increase in annealing temperatures. This confirms the enhancement of films qualities and lower porosities. Further investigations also reveal that in the lower wavelength region up to 390 nm, the refractive index is linearly increased and reached to a peak value and then sharply dropped with the increase in wavelength. Similarly, the k values increase with the increasing of wavelength and reached to the maximum and then fell gradually. These features indicate that n shows normal dispersion in the higher wavelength regions and anomalous dispersions in the lower wavelength sides whereas the inverse phenomena were detected for the k. The dispersion of refractive index exhibits a peak at 3.22 eV (386 nm) corresponding to π–π* transitions of the UV oscillator. On the other hand, the anomalous nature arises due to the resonance effects between incoming solar radiation and electronic polarizability. This leads to the coupling of electrons and oscillating electric fields of the incident electromagnetic radiation. Our observations are consistent with an earlier report.[38] The refractive index is closely related to the electronic polarizability of ions and local filed of inside the films. Estimation of refractive indices of these films are very important for their applications in integrated optical devices such as filters, switches, laser diodes, couplers, lens, detectors and amplifiers. Refractive index is a key parameter for the design of such devices.

Using the single oscillator model suggested by Wemple and DiDomenico *et al.*,[38,39] we present the functional relation for the dispersion of refractive index below the optical band-gap of the films. The dispersion relation of the refractive can be represented by the following terms,[38,39]

$$(n^2-1)^{-1} = \frac{E_0}{E_d} - \frac{1}{E_0 E_d}(h\nu)^2 \quad (9)$$

where E_d is the dispersion energy, a measure of the strength of interband optical transition and E_0 is the single oscillator energy. Fig. 6 shows plots of $(n^2-1)^{-1}$ *vs.* $(h\nu)^2$. The values of E_d and E_0 can be computed from the intercept determined by fitting a straight line to $(\mu^2-1)^{-1}$ axis, (E_0/E_d) and the gradient/slope $(E_0E_d)^{-1}$. The values of the dispersion parameters E_0 and E_d extracted from Fig. 6 are displayed in Table 3. The oscillator parameters E_0 and E_d, dependent on the moments of the optical transitions M_{-1} and M_{-3}, which are defined by the following models,[40]

$$E_0^2 = \frac{M_{-1}}{M_{-3}} \text{ and } E_d^2 = \frac{M_{-1}^3}{M_{-3}} \quad (10)$$

The calculated values of the transition moments M_{-1} and M_{-3} are listed in the following Table 3.

Fig. 6 shows that plots of $(n^2-1)^{-1}$ *vs.* $(h\nu)^2$, for the Cu–Co oxides films before and after annealing, shows that the refractive index values decline towards the longer wavelength regions due to the lattice absorption. From Table 3, it is seen that oscillator energy E_0, transition moments, M_{-1} and M_{-3} decrease with the increase in annealing temperatures while the dispersion energy, E_d, is monotonically enhanced. Dispersion energy

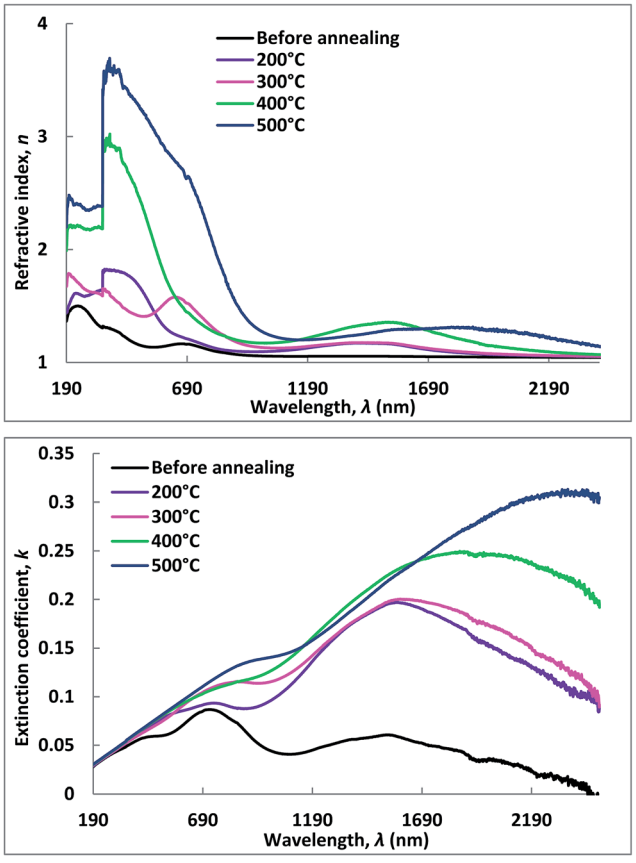

Fig. 5 Real and imaginary parts of the complex refractive index of Cu–Co oxide coatings before and after annealing at different temperatures.

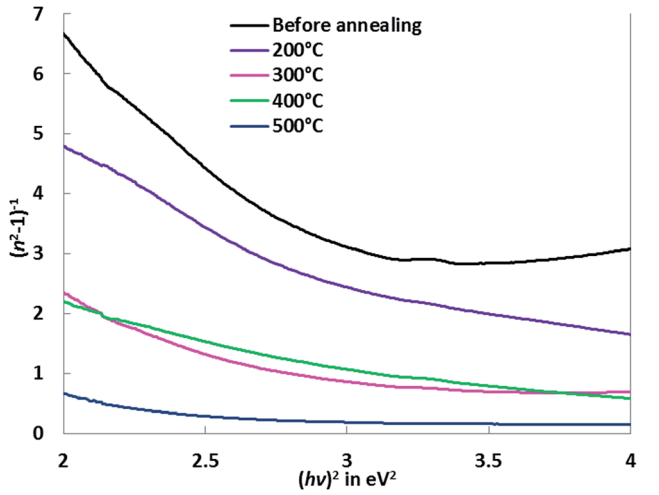

Fig. 6 Plots of $(n^2-1)^{-1}$ *vs.* $(h\nu)^2$ of Cu–Co oxide coatings before and after annealing at different temperatures.

Table 3 Oscillator dispersion parameters, transition moments, oscillator strength and static dielectric constant of Cu–Co oxide coatings before and after annealing at different temperatures

Annealing temperature	Oscillator energy, E_0 (eV)	Dispersion energy, E_d (eV)	Transition moment, M_{-1}	Transition moment, M_{-3} (eV^2)	Oscillator strength, $f = E_0E_d$ (eV^2)	Static dielectric constant, ε_∞
Before annealing	3.96	7.05	2.084	0.175	24.39	3.08
200 °C	3.35	8.75	2.865	0.345	25.20	3.86
300 °C	3.18	9.44	2.433	0.454	25.96	4.43
400 °C	2.87	10.20	3.923	0.580	26.52	4.92
500 °C	2.49	12.15	5.283	0.998	27.95	6.28

measures the intensity of the inter-band optical transition but does not have much effect on the energy band-gap, E_g. The oscillator energy and dispersion energy values are associated with the crystalline structure and ionicity of ionic or covalent materials.[41] This essentially indicates that in addition to the optical characterizations, the single oscillator model can be successfully applied to determine the structural properties of these films.

Furthermore the oscillator strength, f is defined by Wemple and di Domenico for a single oscillator model such as[39]

$$f = E_0E_d \tag{11}$$

The results using the eqn (11) are included in Table 3. The optical dielectric constant at high frequency, ε_∞ also known as the static dielectric constant can be found from the intersection point of the line at $(h\nu)^2 = 0$ while the refractive index at zero photon energy, n_0 (static refractive index) is also related to ε_∞ as, $\varepsilon_\infty = {n_0}^2$. The static dielectric constant is expressed by the following relation,[40]

$${n_0}^2 = \varepsilon_\infty = 1 + \frac{E_d}{E_0} \tag{12}$$

The estimated values of the oscillator strength and static dielectric constants of the Cu–Co oxide coatings before and after being annealed at 200–500 °C are shown in Table 3. Table 3 shows that the oscillator strength and static dielectric constant of the coatings are linearly increased with the gradual increase in annealing temperature of the films. The variation in these optical dispersion parameters and other constants strongly correlated to the thermally driven defects that yield localized states around the energy band-gaps and thereby influence the other optical properties of the films.

3.4 Dielectric characterizations

The frequency dependence of electron excitation spectra of a solid material is defined in terms of complex dielectric function

$$\varepsilon(\omega) = \varepsilon_1(\omega) + i\varepsilon_2(\omega) = (n(\omega) + ik(\omega))^2 \tag{13}$$

where ε_1 and ε_2 are the real and imaginary parts of the dielectric function, respectively are given in terms of the refractive index and extinction coefficient as,[42]

$$\varepsilon_1 = n^2 - k^2 \text{ and } \varepsilon_2 = 2nk \tag{14}$$

Plots of the real and imaginary parts of the dielectric functions as a function of the incident photon energies are given in the following Fig. 7.

In general, the ε_1 and ε_2 values increase with the annealing temperature in the visible and UV-region. A greater ratio between ε_1 and ε_2 demonstrate the thin film coatings having very good low-loss dielectric nature in this frequency range of interest. This is due to the increase in the electron density of the films. In general, the improvement in crystallinity of the film can decrease the degree of electron scattering and increase the free-electron density.[43,44] The fundamental electron excitation

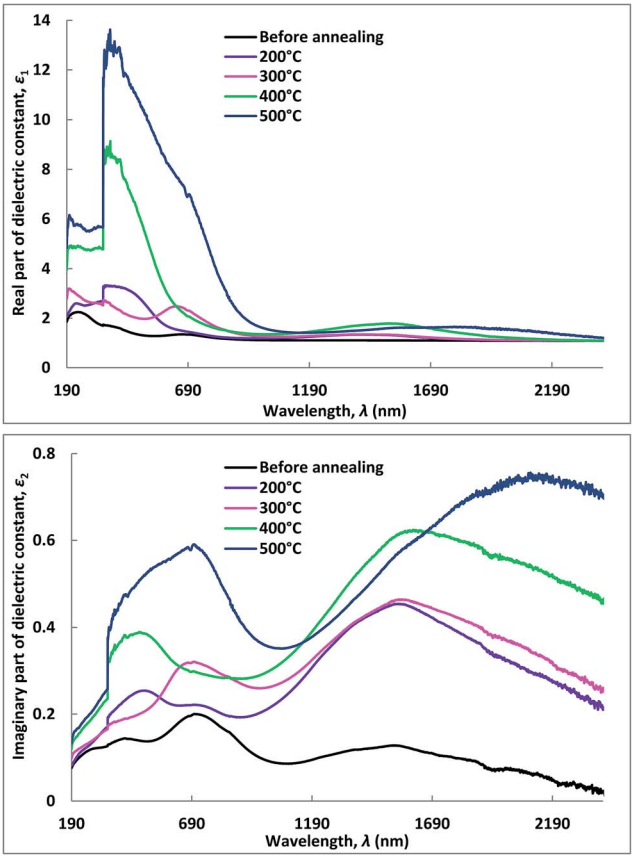

Fig. 7 Real and imaginary part of the dielectric constant *vs.* photon energy of Cu–Co oxide coatings before and after annealing at different temperatures.

spectrum of the thin film was inferred from the frequency dependence of the complex electronic dielectric constant. The frequency response of the dielectric constant signposts the interactions of the photons and electrons in the film is originated in this wavelength range.

In thin film materials, power loss in the form of heat termed as loss factor generally originated from the inelastic scattering process during the charge transfer and charge conduction mechanisms. The ε_1 and ε_2 represent the amount of energy stored in dielectrics as polarization and loss energy, respectively. The power loss factor is associated with electric behaviors of the films and device operations of materials as well. The loss factor is described by,

$$\tan \delta = \frac{\varepsilon_2}{\varepsilon_1} \quad (15)$$

The loss tangent measures the loss-rate of power in a oscillatory dissipative system. Fig. 8 exhibits the variation of the loss factor with the incident photon energy of copper–cobalt oxide thin films before and after being annealed at different temperatures within the range of 200–500 °C. It is clearly seen that the variation loss tangent executes the same trend as ε_2. Since ε_2 is lower than ε_1, then the energy loss of the films is relatively low. This suggests that the films possess good optical qualities due to lower energy losses and lower scattering of the incident radiation. From Fig. 8, it can be seen that in the small photo energy (or low frequency) region (up to 2.0 eV) the loss tangent value of the films increases gradually with the increase of annealing temperatures. However, for photo energy greater than 2.0 eV (or high frequency range), the loss tangent is strongly affected by the annealing temperature.

This feature is associated with the fact that the dipole orientations become minimal at lower temperatures. But as the temperature increases, the orientations of dipoles are facilitated by thermal agitations, consequently the loss tangent increases. It is also assumed that at lower temperatures the conduction loss is minimum and as the temperature increases conduction loss increases as well due to the higher rate of dipole movements.[45] Also from Fig. 8, the energy loss shows a subtle change in magnitude over the whole spectral range. At lower energy sides it shows a maximum value of 0.6 at 0.5 eV, and decreases gradually with the rise in photon energy.

In the dielectric theory, inelastic scattering of electrons in solid films is associated with the energy loss functions. The energy loss functions are known as volume energy loss function, V_{el} and surface energy loss function, S_{el}.[42]

$$V_{el} = \mathrm{Im}\left(-\frac{1}{\varepsilon(\omega)}\right) = \frac{\varepsilon_2}{{\varepsilon_1}^2 + {\varepsilon_2}^2} \quad (16)$$

$$S_{el} = \mathrm{Im}\left(-\frac{1}{\varepsilon(\omega)+1}\right) = \frac{\varepsilon_2}{(1+\varepsilon_1)^2 + {\varepsilon_2}^2} \quad (17)$$

The energy loss functions are related to the optical properties of a material through the real and imaginary parts of dielectric constant. The volume and surface energy loss functions of these coatings before and after annealing at different temperatures are shown in Fig. 9. Both V_{el} and S_{el} follow the same trend as the loss tangent data shown in Fig. 8. It is clear that in the lower frequency regions both functions increase with increasing annealing temperatures. However, in the higher frequency sides (above 1.4 eV), the annealed films exhibit lower loss then the unannealed one and at energies above 2.5 eV both functions become almost constant with further increase in frequency on

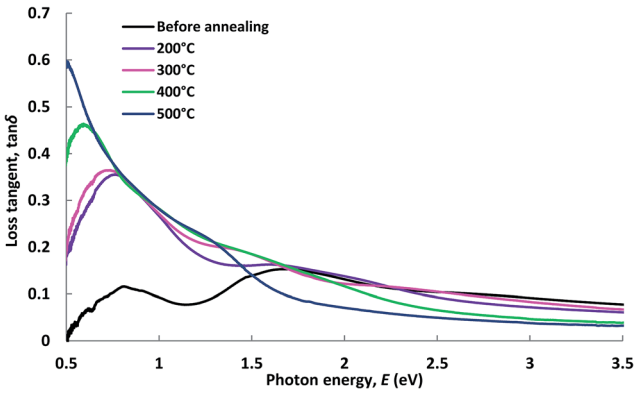

Fig. 8 Loss tangent *vs.* photon energy of Cu–Co oxide coatings before and after being annealed at different temperatures.

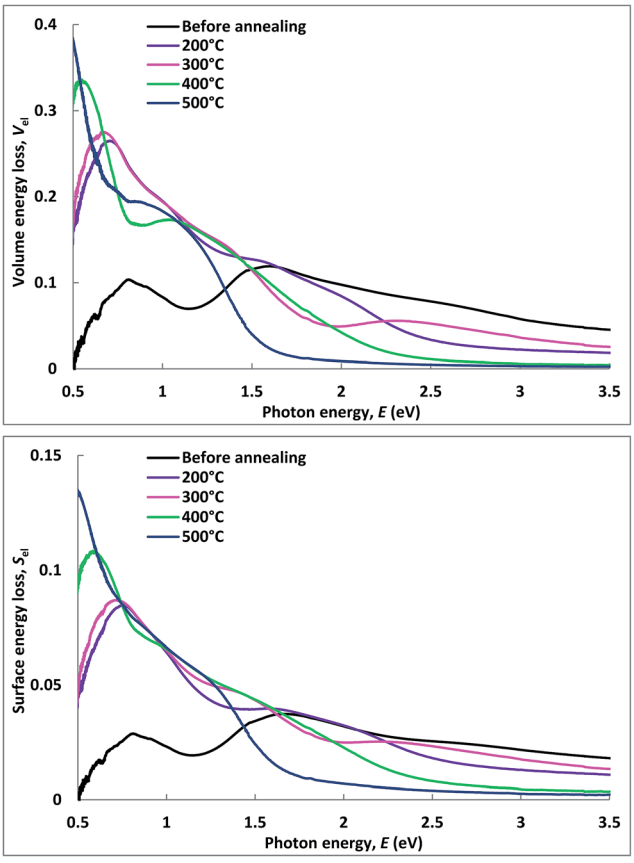

Fig. 9 Variation of volume energy loss and surface energy loss functions of Cu–Co oxide coatings before and after annealing.

the solar spectrum. It is observed that surface energy loss of the films is much lower compared to the value of the volume energy loss functions ($V_{el} > S_{el}$) for any incident photon energies at all annealing conditions. This may indicates that the loss of energy of a free charge carrier when passing through the volume of the film is larger than that when traveling through to the surface of the film. These features are also found to be consistent with previous reports.[46,47] According to Pines and Bohm,[48] due to the excitation of plasma oscillations of conduction electrons, while passing through a medium, specific energy losses are experienced by the fast moving electrons.

3.5 Theoretical predictions

Structural optimization of Cu–Co-oxide ($Cu_{0.5}Co_{2.5}O_4$) system was carried out *via* theoretical modeling. The $Cu_{0.5}Co_{2.5}O_4$ structure exhibits an cubic symmetry in a space group of $Fm\bar{3}m$ (#225) having eight formula units in a unit cell. The lattice constants, in equilibrium condition, of CuCo-oxide systems are 8.29 Å as estimated *via* numerical predictions. These parameters are consistent with that obtained from our previous X-ray diffraction study: $a = 8.09$ Å.[27] In the current cluster model of $Cu_{0.5}Co_{2.5}O_4$, there are 4 Cu, 20 Co and 32 O atoms. The crystal structure was optimized and is shown in Fig. 10.

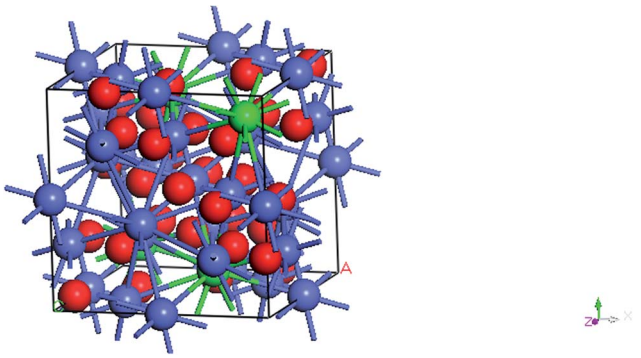

Fig. 10 Conventional unit cell of CuCo-oxide ($Cu_{0.5}Co_{2.5}O_4$) structure.

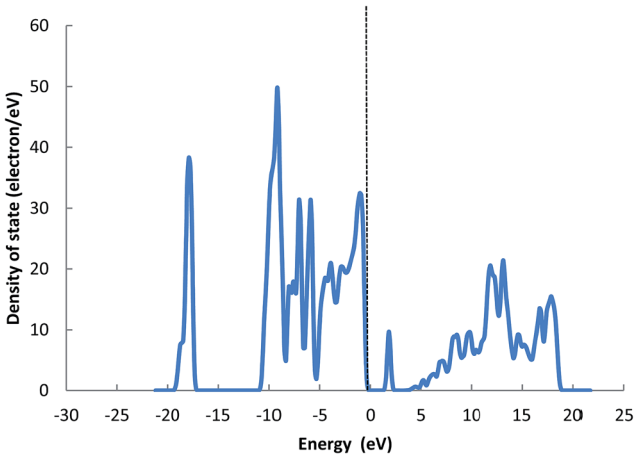

Fig. 11 Total density of states of CuCo-oxide ($Cu_{0.5}Co_{2.5}O_4$) clusters.

Fig. 11 shows the density of states (DOS) for this $Cu_{0.5}Co_{2.5}O_4$ cluster. The electronic properties of the structure were determined *via* computing the total density of states at the Fermi level. The analysis shows that the $Cu_{0.5}Co_{2.5}O_4$ system presents a non-metallic character due to d-orbital of Co and Cu which results in semiconducting nature. The range of the top most valance band is from −11 to 0 eV (Fermi level) and the conduction band above the Fermi level is located at 1.10 eV.

The simulated absorption spectrum of $Cu_{0.5}Co_{2.5}O_4$ system as a function of photon energies in the range of 0.5 to 3.5 eV is shown in Fig. 12. The spectra clearly indicate that the absorption coefficient of this cluster are strongly dependent on the incident energies. Moreover, the absorption coefficient curve confirms that this material exhibits non-metallic nature.[49] Our modeled compound exhibits a good absorption coefficient that can be used to investigate a wider E-M frequency range for promising optical applications.

The dielectric response of a material indicates the interaction between photons and electrons. The energy dependent complex dielectric functions of $Cu_{0.5}Co_{2.5}O_4$ system in the wavelength range of 0 to 2500 nm are displayed in Fig. 13. The calculated dielectric function includes the intra-band effects from free electrons (conduction electrons contribution) and

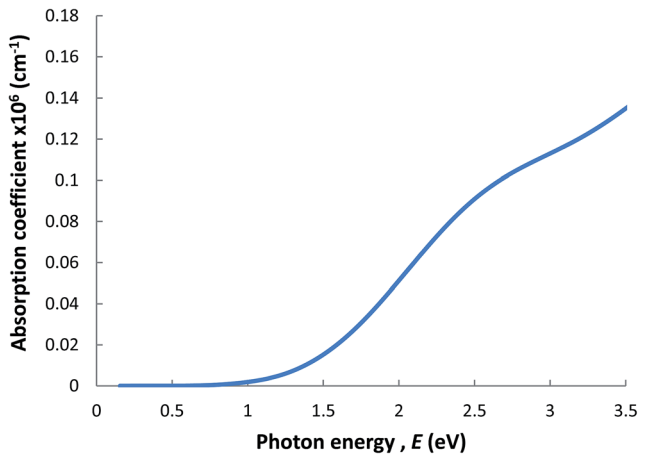

Fig. 12 Theoretical absorption spectrum of $Cu_{0.5}Co_{2.5}O_4$ clusters.

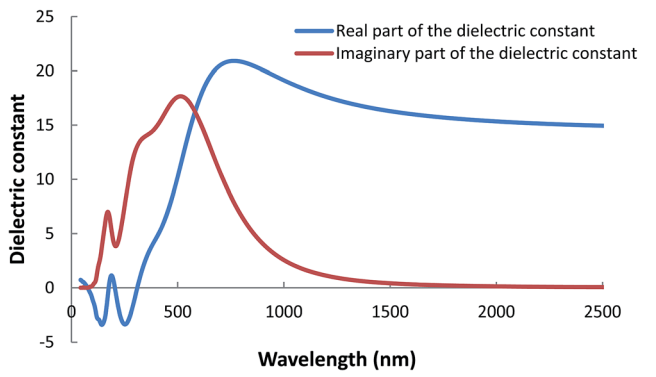

Fig. 13 Real and imaginary parts of dielectric constants of $Cu_{0.5}Co_{2.5}O_4$ clusters.

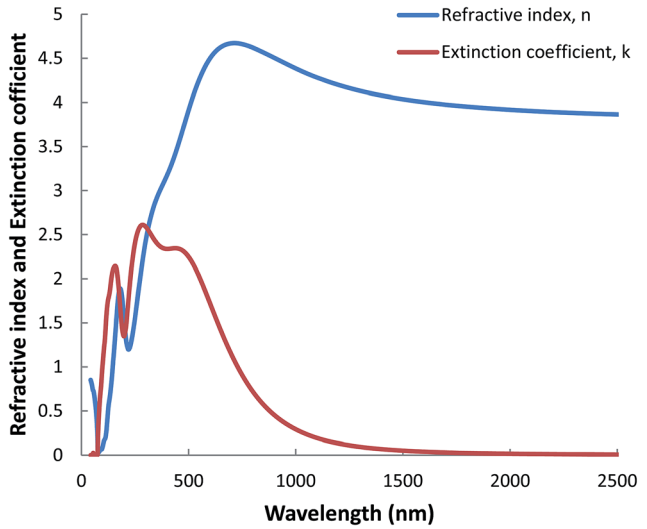

Fig. 14 Refractive index (n) and extinction coefficient (k) spectra of CuCo-oxide coatings.

inter-band effects (from bound-electron contribution). Fig. 13 shows an increasing trend of the dielectric constants at shorter wavelengths which become constant in longer wavelength regions. This can be attributed to the band gap absorption in these coatings. The main peak of imaginary part ε_2 of the dielectric constant is located at 510 nm and reasonably agrees with the experimental results discussed in (Section 3.3). The ε_2 magnitudes reduces to zero in the wavelength range greater than 1600 nm suggesting that this material becomes transparent for longer wavelengths while absorption will occur for nonzero ε_2.[50]

The refractive index (n) and extinction coefficient (k) spectra of such cluster calculated *via* DFT+U modelling, in the wavelength range of 0–2500 nm, are presented in Fig. 14. Similar to the dielectric functions, the refractive index and extinction coefficient plots exhibit maxima in the shorter wavelength regions. The computational and measured refractive index have similar value in the wavelength range from 0 to 2500 nm. Furthermore, the extinction coefficient from the experimental and computational modeling has similar trends but slightly different values. The differences may be due to (i) an ideal situation ($T = 0$ K, $P = 0$ atm), (ii) the mixed phase nature of real films, and (iii) the effect of highly polished Al substrate in the real film materials.

For comparison, we calculate optical properties of a $CoCu_2O_3$ system which can be considered as a metal to oxygen ratio of 3 : 3, while the actual system discussed above is a 3 : 4 metal to oxygen ratio. The $CoCu_2O_3$ system modeling shows similar trends as the $Cu_{0.5}Co_{2.5}O_4$ system. The details for this $CoCu_2O_3$ system are included in the ESI† document.

4. Conclusions

The post-annealing electromagnetic response of optical and dielectric properties of Cu–Co oxide coatings were investigated within the temperature range of 200–500 °C. The optical coefficients such as absorption coefficient, band-gaps, Urbach energy, complex refractive index, optical dispersion parameters; and the dielectric coefficient (such as real and imaginary parts of the complex dielectric constants), loss tangent, and energy loss functions of these coatings were significantly modified by the annealing temperatures up to 500 °C. The refractive index exhibited normal and anomalous dispersions at higher and lower frequencies, respectively. The results based on theoretical modeling of (DFT+U) by the CASTEP Package on $Cu_{0.5}Co_{2.5}O_4$ cluster suggests that the electronic density of states of Cu–Co oxide systems have a semiconducting nature with a band gap ~1.10 eV. The predicted numerical values of the refractive index, extinction coefficient, and complex dielectric functions are in good agreement with the experimental data.

Acknowledgements

M. Mahbubur Rahman gratefully acknowledges the financial support provided by the Murdoch University. Hussein A. Miran thanks the Iraqi government for the award of PhD scholarship.

References

1 L. Yuezin and J. N. Armor, *Appl. Catal., B*, 1993, **3**, L1–L11.
2 N. A. Youssef, M. M. Selim and E. S. Kamel, *Bull. Soc. Chim. Fr.*, 1991, **128**, 648–653.
3 W. M. Shaheen and M. M. Selim, *Thermochim. Acta*, 1998, **322**, 117–128.
4 R. Sundararajan and V. Srinivason, *Recent Developments in Catalysis Technip*, Paris, 1992.
5 Z. Y. Tian, N. Bahlawane, V. Vannier and K. Kohse-Höinghaus, *Proc. Combust. Inst.*, 2013, **34**, 2261–2268.
6 F. Iacomi, G. Calin, C. Scarlat, M. Irimia, C. Doroftei, M. Dobromir, G. G. Rusu, N. Iftimie and A. V. Sandu, *Thin Solid Films*, 2011, **520**, 651–655.
7 E. Ríos, S. Abarca, P. Daccarett, H. Nguyen Cong, D. Martel, J. F. Marco, J. R. Gancedo and J. L. Gautier, *Int. J. Hydrogen Energy*, 2008, **33**, 4945–4954.
8 M. A. Alpuche-Aviles and Y. Wu, *J. Am. Chem. Soc.*, 2009, **131**, 3216–3224.
9 L. Kaluža, B. Orel, G. Dražič and M. Kohl, *Sol. Energy Mater. Sol. Cells*, 2001, **70**, 187–201.
10 L. Kaluža, A. Šurca-Vuk, B. Orel, G. Dražič and P. Pelicon, *J. Sol-Gel Sci. Technol.*, 2001, **20**, 61–83.
11 A. V. Chadwick, S. L. P. Savin, S. Fiddy, R. Alcántara, D. F. Lisbona, P. Lavela, G. F. Ortiz and J. L. Tirado, *J. Phys. Chem. C*, 2007, **111**, 4636–4642.
12 R. Alcántara, M. Jaraba, P. Lavela and J. L. Tirado, *Chem. Mater.*, 2002, **14**, 2847–2848.
13 A. Amri, Z. T. Jiang, T. Pryor, C. Y. Yin, Z. Xie and N. Mondinos, *Surf. Coat. Technol.*, 2012, **207**, 367–374.
14 A. Balland, P. Gannon, M. Deibert, S. Chevalier, G. Caboche and S. Fontana, *Surf. Coat. Technol.*, 2009, **203**, 3291–3296.
15 T. Y. Wei, C. H. Chen, H. C. Chien, S. Y. Lu and C. C. Hu, *Adv. Mater.*, 2010, **22**, 347–351.
16 X. Xiao, L. Miao, G. Xu, L. Lu, Z. Su, N. Wang and S. Tanemura, *Appl. Surf. Sci.*, 2011, **257**, 10729–10736.

17 A. Amri, X. Duan, C. Y. Yin, Z. T. Jiang, M. M. Rahman and T. Pryor, *Appl. Surf. Sci.*, 2013, **275**, 127–135.
18 D. Ding, W. Cai, M. Long, H. Wu and Y. Wu, *Sol. Energy Mater. Sol. Cells*, 2010, **94**, 1578–1581.
19 E. Vila, R. M. Rojas, J. L. Martín De Vidales and O. García-Martínez, *Chem. Mater.*, 1996, **8**, 1078–1083.
20 M. Adsten, R. Joerger, K. Järrendahl and E. Wäckelgård, *Sol. Energy*, 2000, **68**, 325–328.
21 H. C. Barshilia, N. Selvakumar, K. S. Rajam and A. Biswas, *J. Appl. Phys.*, 2008, **103**, 023507.
22 H. J. Brown-Shaklee, W. Carty and D. D. Edwards, *Sol. Energy Mater. Sol. Cells*, 2009, **93**, 1404–1410.
23 P. N. Shelke, Y. B. Khollam, R. R. Hawaldar, S. D. Gunjal, R. R. Udawant, M. T. Sarode, M. G. Takwale and K. C. Mohite, *Fuel*, 2013, **112**, 542–549.
24 A. Amri, Z. T. Jiang, N. Wyatt, C. Y. Yin, N. Mondinos, T. Pryor and M. M. Rahman, *Ceram. Int.*, 2014, **40**, 16569–16575.
25 A. Amri, Z. T. Jiang, P. A. Bahri, C. Y. Yin, X. Zhao, Z. Xie, X. Duan, H. Widjaja, M. M. Rahman and T. Pryor, *J. Phys. Chem. C*, 2013, **117**, 16457–16467.
26 A. Amri, Z. T. Jiang, X. Zhao, Z. Xie, C. Y. Yin, N. Ali, N. Mondinos, M. M. Rahman and D. Habibi, *Surf. Coat. Technol.*, 2014, **239**, 212–221.
27 H. Miran, M. Mahbubur Rahman, Z.-T. Jiang, M. Altarawneh, L. Siang Chuah, H.-L. Lee, E. Mohammedpur, A. Amri, N. Mondinos and B. Z. Dlugogorski, *J. Alloys Compd.*, 2017, **701**, 222–235.
28 S. Dudarev, G. Botton, S. Savrasov, C. Humphreys and A. Sutton, *Phys. Rev. B: Condens. Matter Mater. Phys.*, 1998, **57**, 1505.
29 S. J. Clark, M. D. Segall, C. J. Pickard, P. J. Hasnip, M. I. Probert, K. Refson and M. C. Payne, *Z. Kristallogr. - Cryst. Mater.*, 2005, **220**, 567–570.
30 M. Segall, P. J. Lindan, M. a. Probert, C. Pickard, P. Hasnip, S. Clark and M. Payne, *J. Phys.: Condens. Matter*, 2002, **14**, 2717–2744.
31 D. Vanderbilt, *Phys. Rev. B: Condens. Matter Mater. Phys.*, 1990, **41**, 7892–7895.
32 J. F. Nye, *Physical properties of crystals: their representation by tensors and matrices*, Oxford university press, 1985.
33 Z.-T. Jiang, K. Ohshimo, M. Aoyama and T. Yamaguchi, *Jpn. J. Appl. Phys.*, 1998, **37**, 4008–4013.
34 M. M. Rahman, Z. T. Jiang, P. Munroe, L. S. Chuah, Z. F. Zhou, Z. Xie, C. Y. Yin, K. Ibrahim, A. Amri, H. Kabir, M. M. Haque, N. Mondinos, M. Altarawneh and B. Z. Dlugogorski, *RSC Adv.*, 2016, **6**, 36373–36383.
35 A. Millar, M. M. Rahman and Z.-T. Jiang, *J. Adv. Phys.*, 2014, **3**, 179–193.
36 H. Kabir, M. M. Rahman, T. S. Roy and A. Bhuiyan, *Int. J. Mech. Mechatron. Eng.*, 2012, **12**, 30–34.
37 S. W. Xue, X. T. Zu, W. L. Zhou, H. X. Deng, X. Xiang, L. Zhang and H. Deng, *J. Alloys Compd.*, 2008, **448**, 21–26.
38 A. A. M. Farag and M. Fadel, *Opt. Laser Technol.*, 2013, **45**, 356–363.
39 S. H. Wemple and M. Didomenico Jr, *Phys. Rev. B*, 1970, **1**, 193–202.
40 M. Yıldırım, F. Özel, N. Tuğluoğlu, Ö. F. Yüksel and M. Kuş, *J. Alloys Compd.*, 2016, **666**, 144–152.
41 F. Yakuphanoglu, A. Cukurovali and I. Yilmaz, *Phys. B*, 2004, **353**, 210–216.
42 B. Barış, H. G. Özdemir, N. Tuğluoğlu, S. Karadeniz, Ö. F. Yüksel and Z. Kişnişci, *J. Mater. Sci.: Mater. Electron.*, 2014, **25**, 3586–3593.
43 C. Fournier, O. Bamiduro, H. Mustafa, R. Mundle, R. B. Konda, F. Williams and A. K. Pradhan, *Semicond. Sci. Technol.*, 2008, **23**, 085019.
44 Y. Kim and J. Y. Leem, *Phys. B*, 2015, **476**, 71–76.
45 A. A. Atta, *J. Alloys Compd.*, 2009, **480**, 564–567.
46 H. E. Atyia and N. A. Hegab, *Phys. B*, 2014, **454**, 189–196.
47 S. Sarkar, N. S. Das and K. K. Chattopadhyay, *Solid State Sci.*, 2014, **33**, 58–66.
48 D. Pines and D. Bohm, *Phys. Rev.*, 1952, **85**, 338–353.
49 J. Sun, X.-F. Zhou, Y.-X. Fan, J. Chen, H.-T. Wang, X. Guo, J. He and Y. Tian, *Phys. Rev. B: Condens. Matter Mater. Phys.*, 2006, **73**, 045108.
50 A. Rahman, *et al.*, *J. Adv. Phys.*, 2016, **5**(4), 354.